

Original Article



Role of Gold Nanorods Functionalized by Nucleic Acid Nanostructures Carrying Doxorubicin in Synergistic Anti-Cancer Therapy

Hao Wu^{1,&}, Huangshui Ma^{2,&}, Xinghan Wu³, Qiang Sun², Lin Feng¹, Ruifang Jiang¹,
Yanhong Li^{3,#}, and Quan Shi^{1,#}

1. Department of Stomatology, the First Medical Centre, Chinese PLA General Hospital, Beijing 100853, China; 2. State Key Laboratory of Oral Disease, National Clinical Research Center for Oral Diseases, West China College of Stomatology, Sichuan University, Chengdu 610064, Sichuan, China; 3. NHC Key Laboratory of Comparative Medicine, National Human Diseases Animal Model Resource Center, Beijing Key Laboratory for Animal Models of Emerging and Reemerging Infectious Diseases, National Center of Technology Innovation for Animal Model, Institute of Medical Laboratory Animal Science, CAMS & PUMC, Beijing 100021, China

Abstract

Objective Cancer remains a significant global health challenge, necessitating the development of effective treatment approaches. Developing synergistic therapy can provide a highly promising strategy for anti-cancer treatment through combining the benefits of various mechanisms.

Methods In this study, we developed a synergistic strategy for chemo-photothermal therapy by constructing nanocomposites using gold nanorods (GNRs) and tetrahedral framework nucleic acids (tFNA) loaded with the anti-tumor drug doxorubicin (DOX).

Results Our *in vitro* studies have systematically clarified the anti-cancer behaviors of tFNA-DOX@GNR nanocomposites, characterized by their enhanced cellular uptake and proficient lysosomal escape capabilities. It was found that the key role of tFNA-DOX@GNR nanocomposites in tumor ablation is primarily due to their capacity to induce cytotoxicity in tumor cells *via* a photothermal effect, which generates instantaneous high temperatures. This mechanism introduces various responses in tumor cells, facilitated by the thermal effect and the integrated chemotherapeutic action of DOX. These reactions include the induction of endoplasmic reticulum stress, characterized by elevated reactive oxygen species levels, the promotion of apoptotic cell death, and the suppression of tumor cell proliferation.

Conclusion This work exhibits the potential of synergistic therapy utilizing nanocomposites for cancer treatment and offers a promising avenue for future therapeutic strategies.

Key words: Gold Nanorods; Synergistic therapy; Nanomaterials; Anti-tumor therapy

Biomed Environ Sci, 2025; 38(4): 403-415

doi: [10.3967/bes2024.152](https://doi.org/10.3967/bes2024.152)

ISSN: 0895-3988

www.besjournal.com (full text)

CN: 11-2816/Q

Copyright ©2025 by China CDC

[&]These authors contributed equally to this work.

[#]Correspondence should be addressed to Yanhong Li, Associate Professor, Tel: 86-10-87778141, E-mail: liyanhong8408@163.com; Quan Shi, Associate Professor, Tel: 86-10-66936599, E-mail: shiquan3333@sina.cn

Biographical notes of the first authors: Hao Wu, PhD, M.D., majoring in bio-nanomaterials, E-mail: wh_dds@126.com; Huangshui Ma, Bachelors, majoring in bio-nanomaterials, E-mail: MaHuangsh@163.com

INTRODUCTION

Cancer is a leading cause of death worldwide, with approximately 19.3 million new cases and 10 million deaths reported annually^[1-3]. Therefore, how to effectively treat cancer has become one of the primary concerns in the medical science field. Currently, the main treatment options for cancer include surgery, radiation therapy, and chemotherapy^[4]. However, these traditional methods can have negative effects on patients, such as psychological and physical damage, serious side effects, and multidrug resistance^[5]. In recent years, with fewer side effects compared with traditional methods, nanomaterial-mediated photothermal therapy has attracted attention because of its advantages such as high tumorspecificity, low toxicity, and low invasiveness^[6-9]. The principle of photothermal therapy is that when laser pulses are irradiated on nanoparticles, the temperature of the tumor and elimination of malignant cells can be significantly increased to kill tumor cells through the nonradiative relaxation of nanoparticles and the ionophore resonance effect. Therefore, in order to maximize the anti-tumor effect of photothermal therapy, selecting an effective photothermal agent (photothermal conversion material) is critical^[10-16].

With the advantages of antioxidation and easy modification, gold nanomaterials (GNPs) have become widely applied materials in the synthesis of multifunctional nanomedicine in cancer therapy^[17-19]. GNPs with particular longitudinal surface plasmon resonances (LSPR), defined as gold nanorods (GNRs), can obtain excellent thermal conversion by simply tuning their morphology, and are able to drug load through self-assembly and chemical bonding technology, which greatly expands their application in tumor treatment^[20-24]. However, the effectiveness of photothermal therapy can be weakened in practical treatment due to the thermal tolerance caused by heat shock proteins and the inherent complexity of tumors^[25,26]. Fortunately, the development of nanomedicine offers a potential solution to this issue through the multifunctional modification of GNRs, enabling the implementation of multiple anti-malignant strategies^[19,27]. Doxorubicin (DOX) is a widely used broad-spectrum anticancer drug in clinical treatment, but it has certain drawbacks such as drug resistance, non-selective distribution, and poor permeability, which limit its clinical application^[27,28]. The unique anthracycline-like structure of DOX leads to its ability

to be embedded in the DNA helix in a non-covalent form. Recent studies have demonstrated that DOX can be carried by a biocompatible three-dimensional DNA nanomaterial, enhancing its cellular uptake and drug release capabilities^[29,30].

Inspired by the above progress, our research proposed a strategy of modifying polyethylene glycol (PEG)-modified GNRs to create tFNA-DOX@GNR nanocomposites by utilizing DNA nanostructures to encapsulate the chemotherapeutic agent DOX. These nanocomposites have shown potent anti-cancer effects, with enhanced delivery of DOX to the cell nucleus and improved escape from lysosomal degradation, as illustrated in [Scheme 1](#). The evidence gathered and analyzed in our research indicates that the tFNA-DOX@GNR nanocomposites represent a novel and promising approach to cancer therapy, potentially improving outcomes through integrating photothermal and chemical treatment strategies.

MATERIALS AND METHODS

Materials

All chemicals and solvents applied in this work were at analytical grade. DNA oligos and cyanine 5 (Cy5), termed as single-stranded DNA (ssDNA), were synthesized by HITGEN (Chengdu, China). DOX was purchased from Beyotime (Shanghai, China). The cell counting kit-8 (CCK-8) was purchased from MedChemExpress (Shanghai, China), and PEG-modified GNRs were synthesized in Beijing Zhongkeiming Daojin Technology Co., LTD., using a two-step method. Initially, gold seeds were synthesized by reducing HAuCl₄ solution with AgNO₃. Subsequently, the gold seeds were gradually crystallized into rod-shaped nanostructures in HAuCl₄ solution under specific conditions, followed by the decoration of PEG on the surfaces of the obtained GNRs. The optical absorption peak of GNRs is highly consistent with 808 nm. Other chemicals including Tris-HCl and MgCl₂, were purchased from Aladdin (Shanghai, China).

Preparation of tFNA-DOX and tFNA-DOX@GNR Nanocomposites

The tFNAs were synthesized using four distinct single-stranded DNA (ssDNA) sequences (S1, S2, S3, and S4), with the specific sequences provided in the supporting materials. The synthesis process involved mixing 1 μL of each ssDNA sequence from [Supplementary Table S1](#) with 96 μL of TM buffer

(10×10^{-3} mol/L Tris, 10×10^{-3} mol/L $MgCl_2$; pH = 8.0) and heating the mixture to 95 °C for 10 mins, followed by rapid cooling to 4 °C for 20 mins to form the DNA nanostructures. For the creation of Cy5-labeled tFNAs, S1 strands were substituted with Cy5-S1 strands to enable fluorescence tracking. Subsequently, excessive DOX was incubated with the resulting tFNAs (1 μ mol/L) at 4 °C overnight to yield tFNA-DOX nanocomposites. Removal of Tris-HCl, $MgCl_2$ and excess DOX through ultrafiltration centrifugation using 30-kD ultrafiltration cubes, and the resulting product was stored at 4 °C for subsequent experimentation. This study employed PEG-modified GNRs as the foundational material for further modification. In the synthesis of tFNA-DOX@GNR composites, PEG-modified GNRs were combined with tFNA-DOX nanocomposites in a fixed ratio to produce the final product, which was then stored at 4 °C for subsequent experimentation.

Material Characterization

Polyacrylamide gel electrophoresis (PAGE; 8%) was utilized to confirm the encapsulation of DOX molecules within the tFNA. Transmission electron

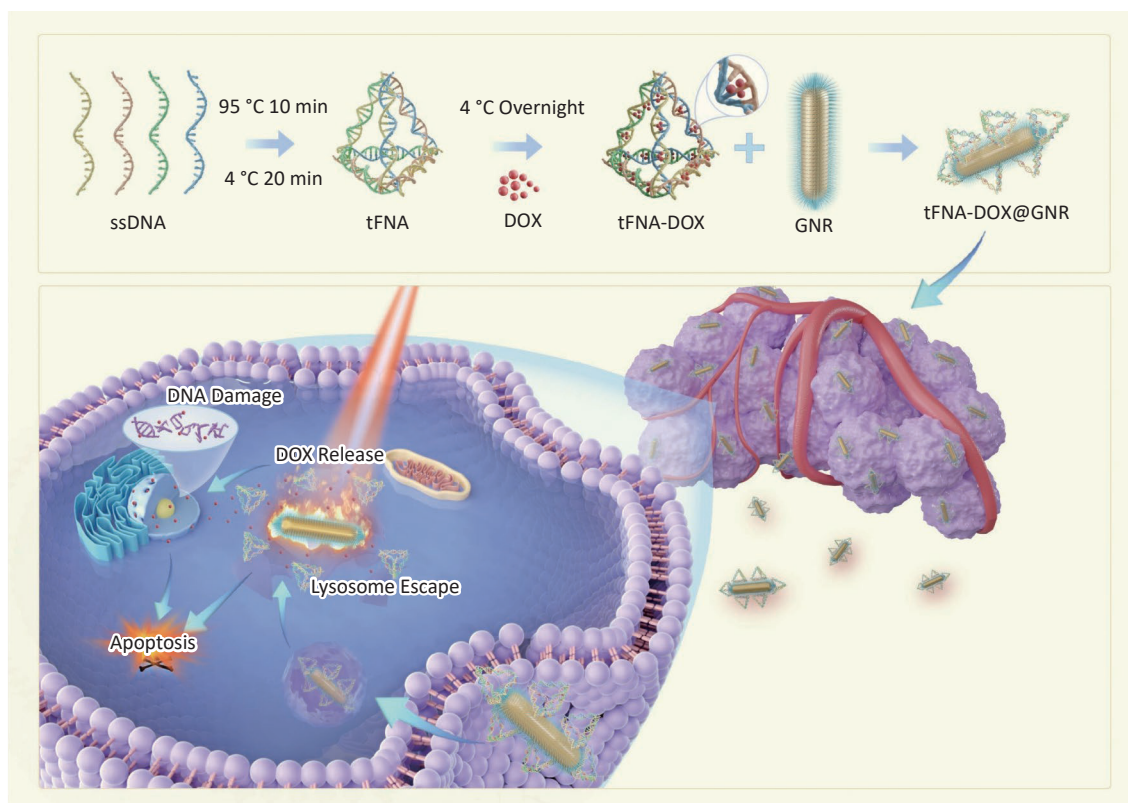
microscopy (TEM, FEI Talos, operated at 200 kV) with an EDS detector was utilized to examine the specific structures, morphology and chemical composition of the nanocomposites. Prior to TEM analysis, specimens of tFNA and tFNA-DOX were negatively stained with a 5% phosphotungstic acid-staining solution for 4 mins.

Zeta Potentials and Hydrated Particle Size Analysis

The Zetasizer from Malvern Instruments Ltd. was used to measure the hydrated particle size and zeta potentials of the different nanostructures obtained during the synthesis procedures using the Dynamic Light Scattering (DLS) method. The tests were conducted at room temperature (25 °C) using 1 mL of the suspension solutions transferred into a centrifugal tube *via* pipette. Prior to testing, the solutions were sonicated in a bath sonicator for 1 h to achieve a homogeneous dispersion.

Photothermal Measurements

Nanocomposite solutions of tFNA-DOX@GNR, with a concentration of 1 mol/L, were subjected to irradiation by an 808-nm laser at various power



Scheme 1. Schematic diagram of the synthesis of nanocomposites and their photothermal-chemotherapy mechanism. ssDNA: DNA single strands; tFNA: tetrahedral framework nucleic acids; GNR: gold nanorods; DOX, Doxorubicin.

densities for a duration of 10 mins. The experimental setup included an 808 nm laser, a thermocouple thermometer, and a data acquisition system. The temperature differential was recorded at 30-s intervals.

Cell Culture

The human melanoma cells (A-375) were cultured in high-glucose DMEM (Hy-Clone) supplemented with 10% fetal bovine serum (FBS) (Corning) and 1% penicillin-streptomycin solution (HyClone) in an incubator at 37 °C with 5% CO₂. Upon reaching 75% confluence, the A-375 cells were passaged using trypsin (HyClone).

Evaluation of Cell Cytotoxicity

For the CCK-8 method to test proliferation viability, A-375 cells, with a cell density of 1×10^4 /mL, were seeded in 96-well plates and incubated for 24 h. Serum-free culture medium containing 10% volume of tFNA-DOX@GNR reagent with various concentrations and blank serum-free culture medium were added to separate wells. Laser irradiation (808 nm, 2.0 W/cm², 10 min) was applied after 4 h of incubation, followed by continued co-incubation for 20 h. After 20 h, CCK-8 reagent was added to the wells and incubated for 2 h in a dark environment. The absorbance value of each well was measured at 450 nm using an enzyme marker, and cell activity was calculated.

For the live/dead cell staining method to evaluate the effect of anti-melanoma cells, A-375 cells with a cell density of 1×10^4 /mL were seeded in 6-well plates and incubated for 24 h. Serum-free culture medium containing 10% volume of tFNA-DOX@GNR reagent (concentration 1 nmol/L) and blank serum-free culture medium were added to separate wells. In the laser-operation groups, laser irradiation (808 nm, 2.0 W/cm², 10 min) was applied after 4 h of incubation, followed by continued co-incubation for 20 h. After centrifugation and removal of the supernatant, the cells were co-incubated with Calcein AM/PI solution for 15 mins. Observation was conducted using a laser-scanning confocal microscope.

Evaluation of Cellular Uptake and Lysosome Escape Ability

A-375 cells were seeded in 6-well plates at a density of 1×10^4 /mL and cultured for 24 h. After discarding the old medium, Cy5-labeled tFNA-DOX@GNR nanomaterials were added, and co-incubation continued for another 24 h. The collected

cells were then stained with Hoechst staining reagent for 30 mins, and the Cy5 and Hoechst staining were observed using fluorescence microscopy. Additionally, cells were inoculated on cell culture slides at a density of 2×10^5 cells per well and cultured for 24 h. After 4, 8, and 12 h of incubation, the medium was discarded, and Cy5-labeled tFNA-DOX@GNR nanomaterials were added. Subsequently, 0.5 mL of Lyso-Tracker Green working solution was added, and the cells were incubated for 1 h at 37 °C. The co-localization of the nanomaterials with cellular lysosomes was observed using two-photon laser confocal microscopy.

Evaluation of Intracellular ROS and CHOP Expression

A-375 cells were seeded in 6-well plates at a density of 2×10^5 cells per mL and cultured for 24 h. After an initial 4-h incubation period, the cells were treated with tFNA-DOX@GNR and incubated for an additional 4 h. Subsequently, the cells were exposed to laser irradiation at a wavelength of 808 nm, with an intensity of 2.0 W/cm², for 10 mins. Following the laser treatment, the cells were further incubated for 20 h.

A-375 cells with a cell density of 2×10^5 cells per mL were seeded in 6-well plates and cultured for 24 h. After an initial 4-h incubation period, the cells were treated with tFNA-DOX@GNR and incubated for an additional 4 h. Subsequently, the cells were exposed to laser irradiation at a wavelength of 808 nm, with an intensity of 2.0 W/cm², for 10 mins. The cells were then incubated for a further 20 h. Following fixation and rinsing, a primary antibody working solution was added to the cells and incubated overnight. After rinsing, an Alexa Fluor 488-labeled secondary antibody working solution was added and the cells were incubated for 1 h at room temperature, protected from light. The cells were then observed and photographed using an inverted fluorescence microscope.

Evaluation of Apoptosis and Cytokines Related to Apoptosis

Cellular proteins were extracted and separated using SDS-PAGE with 7.5%–10% polyacrylamide gels. The separated proteins were then transferred to PVDF membranes and blocked with 5% skim milk. Subsequently, the membranes were incubated overnight at 4 °C with a diluted primary antibody, followed by incubation at room temperature with the secondary antibody. The developed images were captured using a developing solution, and the

grayscale values of the bands were measured and analyzed using Image J software. For the ELISA assay, the cell samples were co-incubated at room temperature (25 °C) using an ELISA kit, and the optical density (OD) values were measured within 5 mins using an enzyme marker.

RESULTS

Materials Synthesis and Characterization

Figure 1A illustrates the synthesis process of tFNA loaded with DOX. Initially, tFNAs were formed by combining four DNA single strands (ssDNA). Subsequently, tFNAs and DOX molecules were mixed and incubated overnight at 4 °C to produce tFNA-DOX nanocomposites. To optimize the drug delivery

capacity, PAGE analysis was conducted to determine the maximum ratio of DOX to tFNA nanostructures, as displayed in Figure 1B. This step ensured the efficient loading of DOX onto the tFNA nanocomposites and demonstrated that tFNAs loaded with DOX exhibit slower movement compared to tFNA alone, indicating the successful synthesis of tFNA-DOX nanocomposites. The analysis reveals that the maximum ratio of DOX to tFNA combination is approximately 25, suggesting that each tFNA nanostructure can accommodate at least 20 DOX molecules. However, when the ratio exceeds 25, the stability of the resulting tFNA-DOX nanocomposites in the buffer environment becomes compromised.

Transmission electron microscopy (TEM) was used to observe the morphology of various

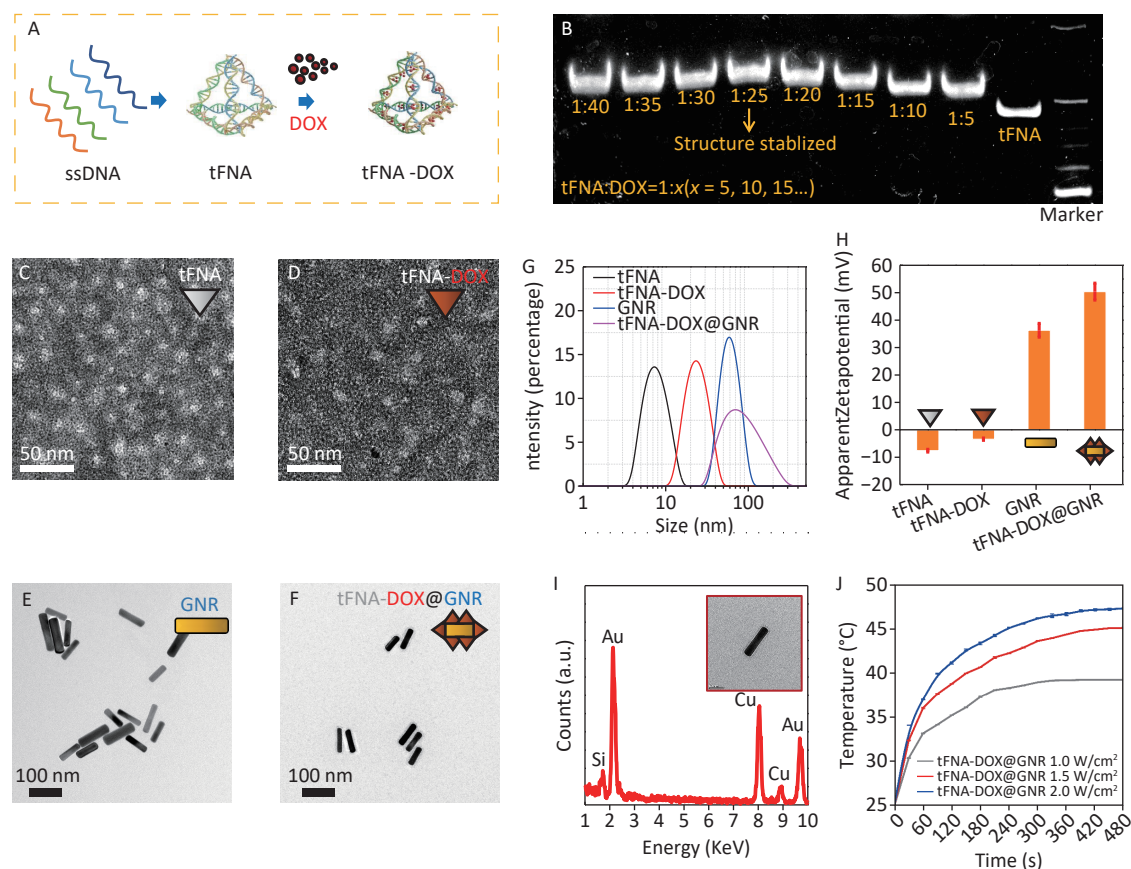


Figure 1. Preparation and characterization of tFNA-DOX@GNR: (A) schematic illustration of the preparation of the tFNA-DOX nanocomposite; (B) PAGE analysis of the tFNA-DOX nanocomposite with different tFNA:DOX ratios; (C–F) TEM investigations of tFNA, tFNA-DOX, GNR and tFNA-DOX@GNR nanostructures, respectively; (G) hydrodynamic diameter distributions of tFNA, tFNA-DOX, GNR, and tFNA-DOX@GNR, respectively, via the DLS method; (H) Zeta potentials of tFNA, tFNA-DOX, GNR, and tFNA-DOX@GNR, respectively; (I) EDS analysis performed on GNR, showing the chemical composition; (J) photothermal heating curves of tFNA-DOX@GNR under different laser irradiation conditions. ssDNA: DNA single strands; tFNA: tetrahedral framework nucleic acids; GNR: gold nanorods; DOX, Doxorubicin.

nanostructures, including tFNA, tFNA-DOX, GNR, and tFNA-DOX@GNR, as depicted in [Figure 1C–1F](#) and [Supplementary Figure S1A](#). [Figure 1C](#) displays triangular-shaped nanostructures, which correspond to the projections of tFNA nanostructures. The morphology of the tFNA-DOX nanocomposite, shown in [Figure 1D](#), exhibits a larger size compared to tFNAs due to the incorporation of DOX. [Figure 1E](#) and [Figure 1F](#) present images of GNR and tFNA-DOX@GNR, respectively. Notably, tFNA-DOX@GNR is observed to be enveloped by electron-transport nanostructures, indicating the successful anchoring of tFNA-DOX nanocomposites onto the surfaces of PEG-modified GNR. To further understand the synthesis process of tFNA-DOX@GNR nanocomposites, [Figure 1G](#) presents the hydrodynamic diameter of tFNA, tFNA-DOX, GNR, and tFNA-DOX@GNR, which is consistent with the findings from TEM investigations ([Supplementary Figure S1B](#)).

[Figure 1H](#) displays the Zeta potentials of tFNA, tFNA-DOX, GNR, and tFNA-DOX@GNR, indicating that the tFNA-DOX@GNR nanocomposites exhibit excellent stability due to their well-designed structure. [Figure 1I](#) shows the EDS spectrum obtained from GNR in the TEM investigation, confirming the presence of Au, while the signals of C and Cu originate from the carbon film on the TEM grid supported by copper grids. To demonstrate the thermal heating capability of the obtained tFNA-DOX@GNR, experiments were conducted using tFNA-DOX@GNR with a concentration of 1 nmol/L under three different power densities with an 808 nm laser ([Supplementary Figure S2](#)), as displayed in [Figure 1J](#). The results indicate that a temperature exceeding 40 °C can be easily achieved by adjusting the concentration or power density of laser irradiation. Therefore, these nanocomposites are promising for application in photothermal tumor therapy. In addition, by simply modifying the delivered drugs, this platform can be applied to photothermal antibacterial therapy, utilizing the heating effect from gold nanorods and the delivery of antibiotics.

To assess the anti-tumor efficacy of the tFNA-DOX@GNR nanocomposites, [Figure 2A](#) displays the staining of live and dead A375 cells, a type of human melanoma cell line. After 24 h of total incubation, the experimental group with tFNA-DOX@GNR nanocomposites but without near-infrared (NIR) laser irradiation showed a modest amount of fluorescent red signal, attributed to the introduction of DOX. In contrast, the experimental group with NIR

irradiation exhibited significantly enhanced fluorescent red signals, indicating a notably increased killing effect of nanocomposites induced by photothermal therapy. The corresponding quantitative analysis of the fluorescence intensity is presented in [Figures 2B](#) and [2C](#).

[Figure 2D](#) evaluates the cytotoxicity of tFNA-DOX@GNR nanomaterials on A-375 cells at various concentrations using the CCK-8 array method, demonstrating a decrease in cell viability with increasing concentrations of the nanomaterials. Additionally, [Figure 2E](#) assesses the ability of tFNA-DOX@GNR nanomaterials to inhibit the proliferation of A-375 cells. In the absence of NIR laser treatment, tFNA-DOX@GNR effectively reduced the cell viability of A-375 cells. Furthermore, the inhibitory effect of tFNA-DOX@GNR on the viability of A-375 cells was enhanced by NIR laser treatment, consistent with the live-dead staining analysis, indicating that the tFNA-DOX@GNR nanocomposites can be an effective anti-tumor strategy.

Cellular Uptake and Lysosome Escape Behavior

To investigate the tumor cell uptake and intracellular transport behavior of tFNA-DOX@GNR nanocomposites, [Figure 3](#) shows their cellular uptake and lysosomal escape effect, which can determine the effectiveness of delivering their anti-tumor payload to the tumor cells. As illustrated in [Figure 3A](#), we employed Cy5 modification on tFNA-DOX@GNR and conducted a fluorescence assay for localization. [Figure 3B](#) shows that the red fluorescence (representing the locations of nanomaterials) gradually overlapped with the blue fluorescence (representing nuclei) as the incubation time increased. This observation suggests that the tFNA-DOX@GNR nanocomposites have good cellular uptake ability and exhibit good binding ability with the nucleus. In addition, the ability of nanodrugs to escape from lysosomes is a crucial factor in effectively killing tumor cells^[31]. In [Figure 3C](#), following a 4-hour co-incubation of tumor cells with tFNA-DOX@GNR, a yellow fluorescence signal was observed within the cells. This signal resulted from the overlap between the red fluorescence emitted by Cy5-labeled nanomaterials and the green fluorescence originating from intracellular lysosomes, indicating that the tFNA-DOX@GNR nanocomposite can partially escape from the lysosomes at 4 h. After 8 h of co-incubation, the yellow fluorescence signal from the overlapping red and green fluorescence was reduced, and a clear separation of red and green fluorescence could be

observed. Furthermore, the yellow fluorescence diminished after 12 h of co-incubation, and the distinct separation of green and red fluorescence signals became more pronounced, suggesting that, starting from 8 h of incubation. Therefore, the tFNA-DOX@GNR nanocomposites successfully escaped from lysosomes, suggesting that they can facilitate drug entry into the nucleus and promote the anti-tumor effect.

Expression of Intracellular ROS and CHOP

Reactive oxygen species (ROS) and CHOP play crucial roles in cellular injury under cellular stress conditions. Excessive ROS accumulation can trigger endoplasmic reticulum stress, leading to apoptosis. Additionally, CHOP acts as a significant cytokine in the endoplasmic reticulum stress pathway, promoting pro-apoptotic effects^[32,33]. Inspired by

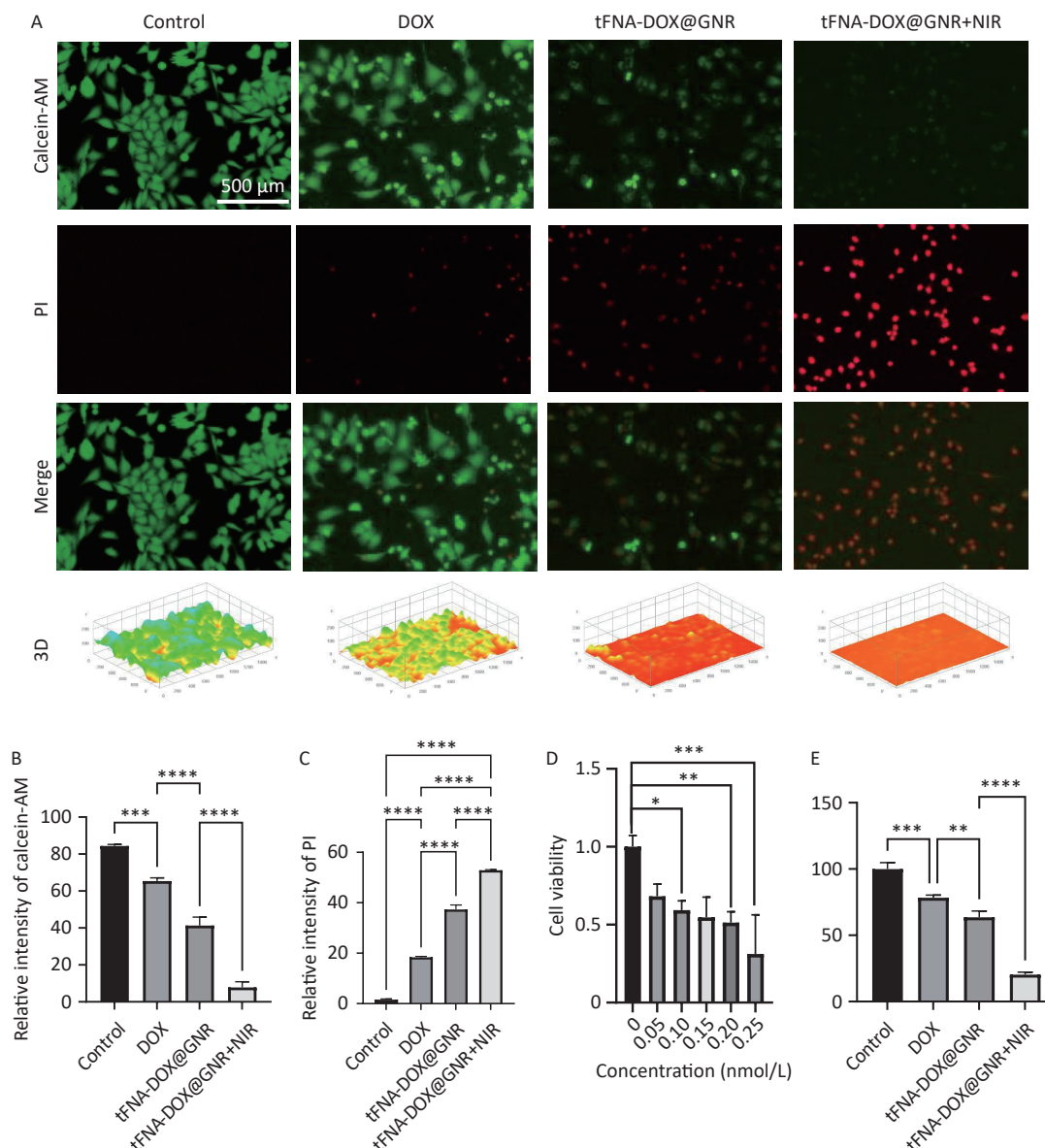


Figure 2. *In vitro* antitumor efficacy evaluation of tFNA-DOX@GNR. (A) Live/dead viability/cytotoxicity assay of tFNA-DOX@GNR and tFNA-DOX@GNR+NIR laser irradiation in A-375 cells and (B, C) the corresponding quantitative analysis of fluorescence intensity; (D) the cytotoxicity of tFNA-DOX@GNR in A-375 cells with different concentrations; (E) *in vitro* cytotoxicity of tFNA-DOX@GNR and tFNA-DOX@GNR+NIR laser irradiation in A-375 cells. tFNA: tetrahedral framework nucleic acids; GNR: gold nanorods; DOX, Doxorubicin; NIR: near-infrared.

these factors, we investigated the generation of intracellular ROS and CHOP induced by tFNA-DOX@GNR nanocomposites. Figures 4A and 4C display the CHOP fluorescence signals of the stained A-375 cells after co-incubation. The figures indicate that the experimental group using the tFNA-DOX@GNR nanocomposite exhibited a higher green fluorescence signal compared to the control group, regardless of NIR irradiation. However, when NIR irradiation was not applied, the experimental group using the tFNA-DOX@GNR nanocomposite alone showed only limited enhancement of fluorescence signal. The quantitative analysis of mean optical density confirmed that the tFNA-DOX@GNR+NIR experimental group exhibited an increase in fluorescence intensity compared to the other three groups ($P < 0.05$), indicating tFNA-DOX@GNR can effectively induce pro-apoptotic effects. Figures 4B and 4D displayed the ROS fluorescence signal of the

stained A-375 cells after co-incubation. It is evident that in the experimental group using tFNA-DOX@GNR nanocomposites without NIR irradiation, there was a slight increase in green fluorescence signal compared to the control group, but the difference was not significant. As shown, the tFNA-DOX@GNR+NIR experimental group showed a significant increase in green fluorescence signal compared to the other three groups ($P < 0.05$), indicating our obtained nanocomposites can increase ROS accumulation and involvement in boosting endoplasmic reticulum stress, leading to apoptosis.

Expression of Cytokines Related to Apoptosis and Pyroptosis

Caspase-1 and caspase-3 are representative members of the caspase family, with caspase-1 being associated with apoptosis and caspase-3 playing a

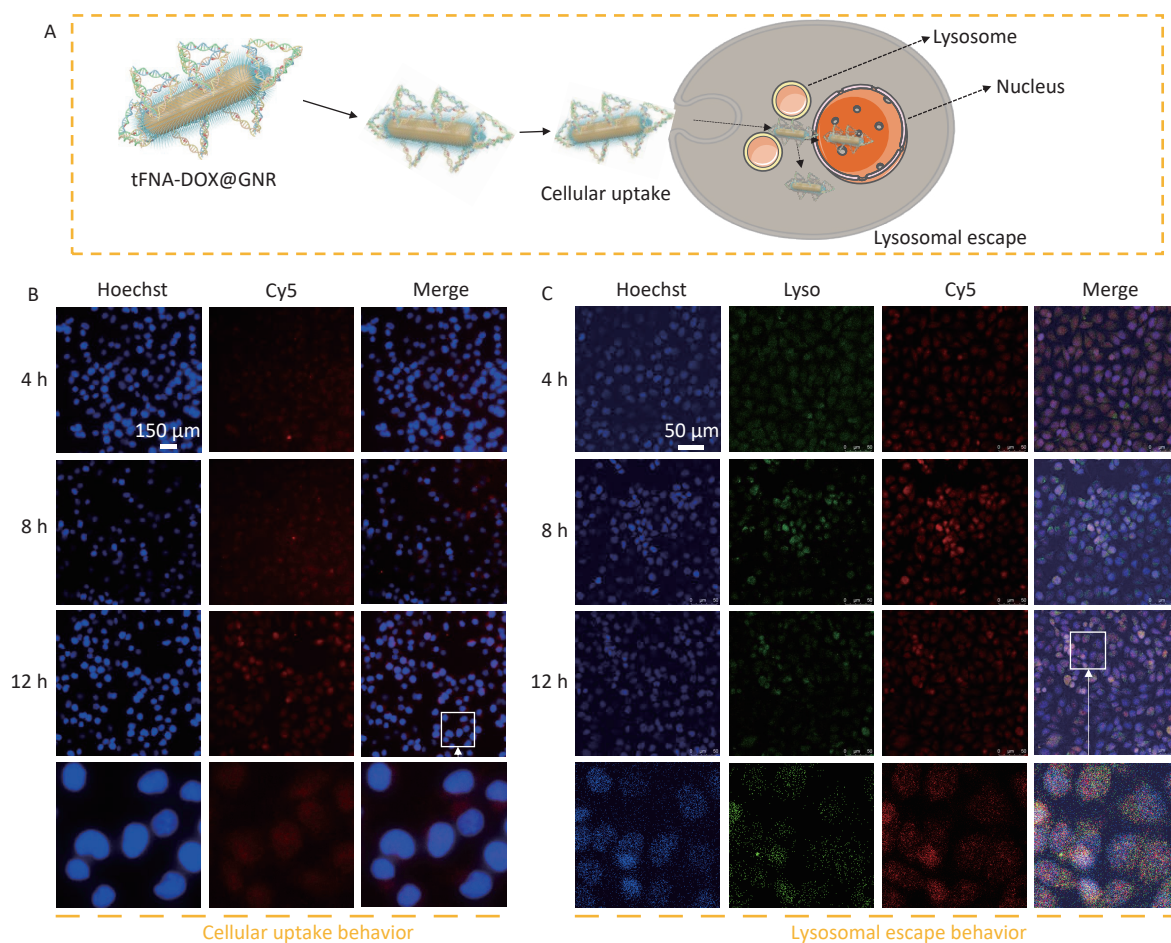


Figure 3. Cellular uptake and lysosome escape behavior. (A) Schematic illustration of the behaviors of tFNA-DOX@GNR nanocomposites; (B) fluorescence microscopy image showing the cellular uptake of tFNA-DOX@GNR nanocomposites in A-375 cells; (C) fluorescence microscopy image demonstrating the lysosomal escape effect of tFNA-DOX@GNR nanocomposites on A-375 cells.

crucial role in mediating apoptosis. They share homology as proteins within the caspase family^[34]. BAX and BCL-2 belong to the same family, in which BCL-2 is an anti-apoptotic protein; when BCL-2 is highly expressed, it can form a heterodimer with BAX and inhibit apoptosis. In contrast, BAX is a pro-apoptotic protein; when intracellular BAX is highly expressed, it promotes cell apoptosis^[35]. GSDME is a member of the gasdermin family that promotes the activation of pyroptosis^[36]. In this work, to confirm the presence of apoptosis and pyroptosis induced by tFNA-DOX@GNR nanocomposites, the levels of caspase-1, caspase-3, BAX, and GSDME were examined. Figures 5A and 5B demonstrate that these protein levels were upregulated in the tFNA-DOX@GNR experimental group, and significant statistical differences were observed compared to the control group. Furthermore, in the tFNA-DOX@GNR+NIR experimental group, the expression

levels of these proteins were even more significantly upregulated. In addition, Figures 5C and 5D demonstrate that both experimental groups with tFNA-DOX@GNR showed different levels of IL-1 β and IL-18. The tFNA-DOX@GNR+NIR group showed more significant upregulation than the experimental group with tFNA-DOX@GNR alone, and there was also a statistical difference with the control group. Therefore, the designed tFNA-DOX@GNR nanocomposites can significantly induce the expression of cytokines related to apoptosis and pyroptosis under laser irradiation.

DISCUSSION

Our previous studies verified the biosafety of DNA-functionalized GNR nanocomposites for normal cells^[37]. It was observed that the combined application of tFNA-DOX@GNR and NIR irradiation

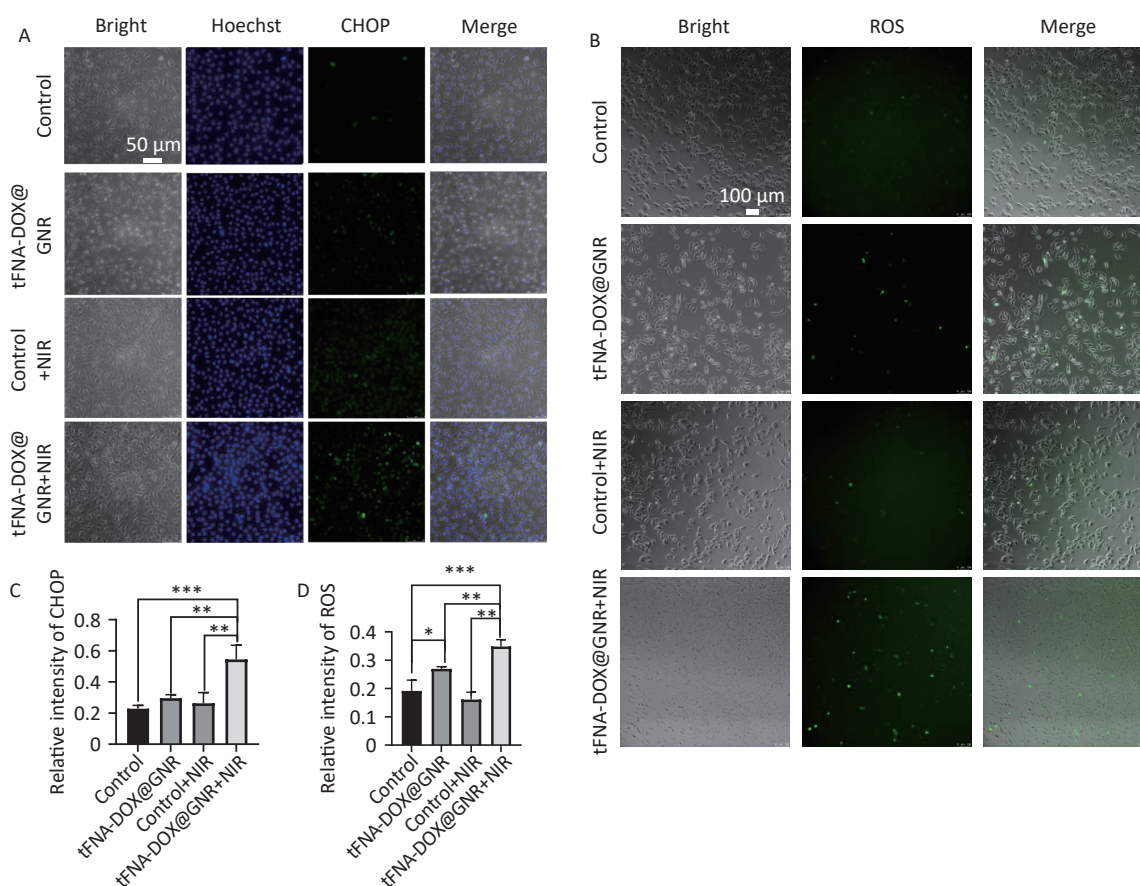


Figure 4. Expression of intracellular ROS and CHOP. (A) and (C) Fluorescence microscopy images and quantitative analysis of CHOP protein expression in A-375 cells treated with tFNA-DOX@GNR nanocomposites under different conditions; (B) and (D) fluorescence microscopy images and quantitative analysis of ROS expression in A-375 cells treated with tFNA-DOX@GNR nanocomposites under different conditions.

resulted in a synergistic photothermal-chemical killing effect, which was efficacious in A-375 cells. Thus, we further focused on the fundamental mechanism of tFNA-DOX@GNR in anti-tumor therapy and clarified the behavior of taking the effects in this study.

In previous years, numerous studies have reported that a rapid increase in local temperature (approximately 42 °C to 45 °C) can effectively kill tumor cells^[38], thereby ensuring biosafety and enhancing anti-tumor efficacy^[39]. It has been well demonstrated that laser irradiation (e.g. 808 nm, 1.0 W/cm²) for a couple of minutes could elevate the temperature of GNR within the tFNA-DOX@GNR nanocomposite to 42 °C, resulting in effective tumor cell eradication. The tFNA-DOX nanocomposite

possesses a high binding capacity for DOX molecules due to its tFNA nanostructure and exhibits excellent endocytosis ability. Consequently, tFNA-DOX can further enhance the transport capacity of DOX molecules, thereby achieving a potent inhibitory effect on tumor cells through chemotherapy.

The investigation on the intracellular localization of tFNA-DOX@GNR nanocomposites revealed their remarkable ability to enter cells, with a notable tendency to accumulate within the nucleus. This finding suggests that tFNA-DOX@GNR nanocomposites hold great potential as nano-drug carriers for enhancing the efficacy of tumor-killing drugs. The exceptional cell entry ability observed in this study can be attributed to the delivery medium, tFNA, utilized in the construction of the tFNA-

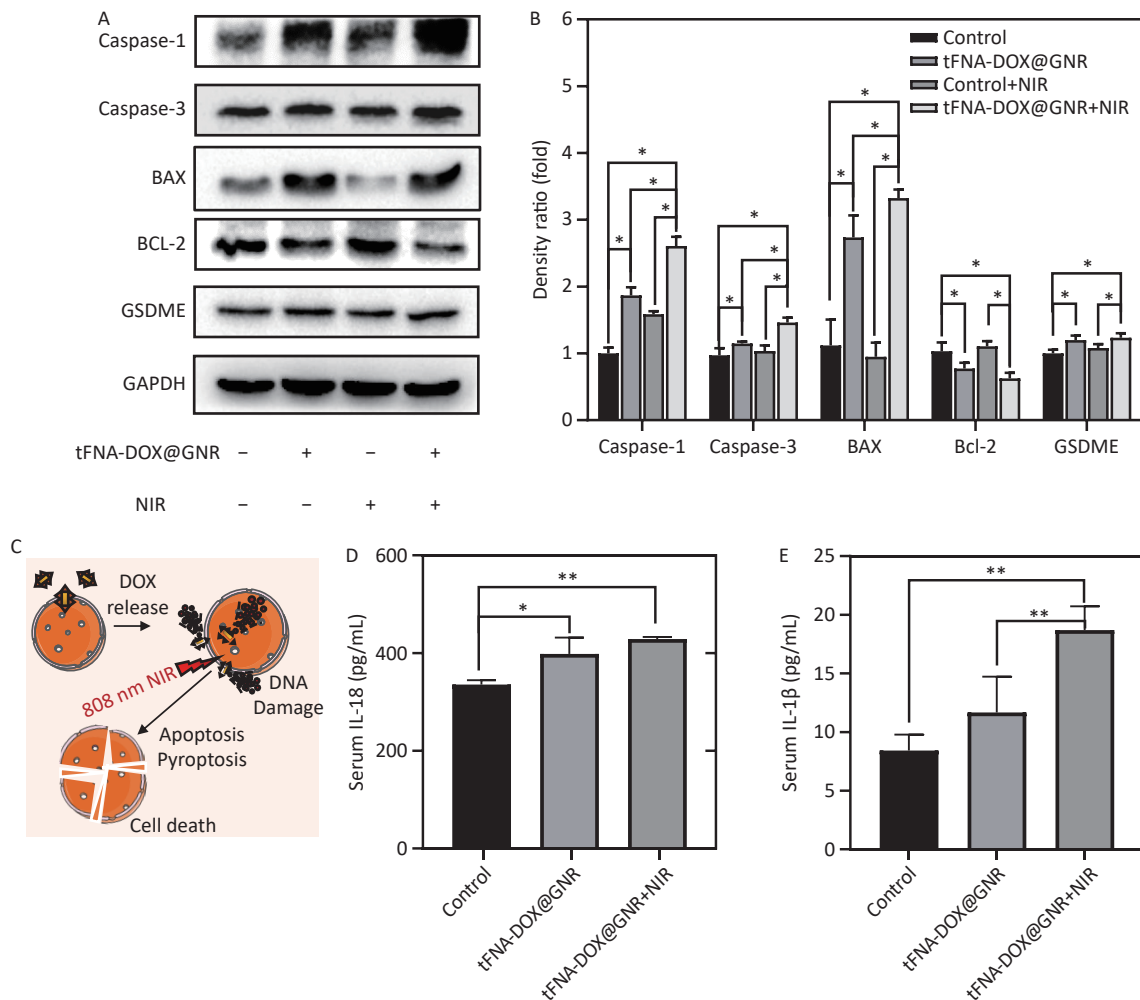


Figure 5. Expression of cytokines related to apoptosis and pyroptosis. (A) and (B) Expression level and semi-quantitative analysis of tFNA-DOX@GNR on apoptosis/pyroptosis-related proteins in A-375 cells tested by Western Blot; (C) schematic illustration of the anti-tumor mechanism of tFNA-DOX@GNR; (D-E) effect of tFNA-DOX@GNR on the expression levels of IL-1β and IL-18 in A-375 cells tested by ELISA.

DOX@GNR nanocomposites. Interestingly, our study demonstrated that tFNA can autonomously penetrate cells in large quantities, irrespective of their surface charge, even in the absence of functional molecules^[40]. Various theories have put forth different explanations regarding the cell membrane penetration ability of tFNA. Among these, a widely accepted explanation proposes that tFNA is capable of reorienting itself in three-dimensional space. By positioning the apex of its tetrahedral structure towards the cell membrane, it effectively reduces electrostatic repulsion. Consequently, tFNA can enter the cell through foveolar protein-mediated endocytosis^[41]. Thus, tFNA may have mediated the cell entry behavior of GNR-based nanocomposites in this study.

The effective escape of nanomaterials from the lysosome to the cytoplasm, following their penetration of the cell membrane and entry into the cell, is crucial for effective drug delivery and the eradication of tumor cells. It has been observed that tFNA-DOX nanocomposites typically undergo decomposition within the lysosomes of cells^[42]. The investigation on the intracellular localization of tFNA-DOX@GNR nanocomposite revealed that it has a strong ability to enter cells and tends to accumulate in the nucleus. Experiments on lysosomal escape showed that tumor cells exhibited escape from lysosomes after 4 h of co-incubation with tFNA-DOX@GNR, and notably entered the nucleus after 8 h. This suggests that the nanocomposite has a good ability to escape from lysosomes. We believe that the lysosomal escape mechanism of tFNA-DOX@GNR nanocomposites primarily relies on the surface properties of the nanostructures of GNR treated with PEG in this study. The negatively charged PEG-treated GNR surface absorbs a significant amount of H⁺ ions from the acidic lysosomal environment, resulting in the "proton sponge effect". This effect leads to changes in lysosomal osmotic pressure and the release of lysosomal contents into the cytoplasm, enabling successful escape from the lysosomes^[43]. The lysosomal escape ability of nanocomposites facilitates the entry of drugs into the cell nucleus and promotes anti-tumor effects.

The mechanism of tumor cell death induced by photothermal-chemical killing is complex, and existing studies suggest that apoptotic pathways mediated by residual heat and chemotherapeutic drugs inside and outside the cells are important mechanisms for their anti-tumor effects, which include various pathways such as the endoplasmic

reticulum stress pathway and oxidative stress pathway^[44]. Acute and high levels of ROS can induce cell death by causing oxidative stress, which leads to alterations in the structure of proteins, lipids, and DNA. While normal cells can withstand the effects of the same concentration of ROS, tumor cells are more prone to cell death due to three factors: elevated intracellular ROS levels, increased susceptibility to ROS due to unstable cell structure, and impaired oxidative stress defense mechanisms^[45]. Oxidative stress in tumor cells activates the endoplasmic reticulum stress response pathway, which in turn activates CHOP by initiating the unfolded protein response. CHOP is a key specific transcription factor of the endoplasmic reticulum stress-initiated apoptotic pathway that regulates multiple downstream apoptotic mechanisms^[46].

In the present study, the fluorescence signals of ROS and CHOP were significantly enhanced in the tFNA-DOX@GNR+NIR group, indicating that the photothermal-chemical synergism of tFNA-DOX@GNR could potentially cause cellular stress injury in A-375 cells, possibly inducing apoptosis through ROS-mediated oxidative overstimulation and endoplasmic reticulum stress. BAX/BCL-2 is a pair of homologous apoptosis-associated proteins. BAX can be upregulated due to high CHOP expression, which can promote mitochondrial cytochrome C release, apoptotic vesicle formation, and caspase activation, leading to apoptosis^[47]. In contrast, Bcl-2 can form a dimer with BAX and inhibit the formation of BAX homodimers. When BAX is overexpressed, it promotes cell death. Caspase-3 can be directly involved in apoptosis execution and is a key protein in mediating apoptosis^[48]. Therefore, the photothermal-chemical synergy of tFNA-DOX@GNR in this study led to the upregulation of BAX expression and the downregulation of BCL-2 expression. This led to BAX/Bcl-2 ratio upregulation and caused a significant increase in caspase-3 expression, thus promoting apoptosis. Pyroptosis is a new mode of programmed cell death discovered in recent years that is mainly caused by inflammatory vesicles, leading to the activation of inflammatory cytokines and eventually inducing cell death by swelling and rupture^[49]. GSDME is a member of the gasdermins family of proteins, which are key effector molecules of pyroptosis. GSDME can be cleaved and activated by caspase-3, switching caspase-3-mediated apoptosis to pyroptosis, thus making cancer cells more sensitive to chemical anti-tumor drugs. Caspase-1 is an important cytokine in the pyroptosis pathway. Caspase-1 is activated by

inflammatory vesicles such as NLRP3, NLRC4, AIM2, and pyrin, which cleave GSDMD proteins to promote cell death and cleave and activate inflammatory factors such as IL-18 and IL-1 β , which are then released extracellularly to amplify the inflammatory response^[50]. The results presented in this work confirmed that the photothermal-chemical synergistic effect of tFNA-DOX@GNR promoted pyroptosis by increasing the expression level of related cytokines, thereby enhancing anti-tumor therapy.

CONCLUSION

In the present study, we introduce a novel nanocomposite, tFNA-DOX@GNR, which was designed for synthetic anti-tumor therapy through the augmentation of apoptosis and pyroptosis pathways. Our research systematically investigates the role of this nanocomposite, showing its capacity to effectively deliver chemotherapeutic agents into tumor cells and enhancing its effectiveness in killing tumors as photothermal agents. In addition, this nanocomposite has demonstrated the ability to escape from lysosomes. The mechanism of tumor destruction observed in this work primarily involves direct killing through the rapid generation of high temperatures *via* a photothermal effect and introduced chemotherapeutic drugs. The construction strategies developed in this study for multifunctional nanomedicine could be applied to the design of novel nanomedicine components for the effective treatment of oral tumors.

Funding This work was supported by the PLAGH Innovation Funds, (Grant No. 22QNFC080); the Sichuan Science and Technology Program (Grant No. 2023ZYD0064 and 2023YFG0220); the Fundamental Research Funds for the Central Universities (Grant No. YJ202242); the Research Funding from West China School/Hospital of Stomatology; Sichuan University (Grant No. QDJF2022-2); and National Undergraduate Training Program for Innovation (Grant No. C2024129736).

Competing Interests All authors declare no conflicts of interest.

Ethics This study is exempt from ethical review.

Authors' Contributions Experimental design, experiment execution, and manuscript drafting: Hao Wu and Huangshui Ma; Material synthesis and analysis: Huangshui Ma, Lin Feng, and Qiang Sun; Biological experiments: Hao Wu, Xinghan Wu, and Ruifang Jiang; Project supervision and manuscript

revision: Quan Shi and Yanhong Li.

Received: June 14, 2024;

Accepted: August 12, 2024

REFERENCES

- Sung H, Ferlay J, Siegel RL, et al. Global cancer statistics 2020: GLOBOCAN estimates of incidence and mortality worldwide for 36 cancers in 185 countries. *CA Cancer J Clin*, 2021; 71, 209–49.
- Liang GH, Cao WQ, Tang DS, et al. Nanomedomics. *ACS Nano*, 2024; 18, 10979–1024.
- Guo H, Hou YC, Wang CX, et al. How to optimize the immune checkpoint blockade therapy for cancers? *Oncologie*, 2024; 26, 343–8.
- Epstein JB, Thariat J, Bensadoun RJ, et al. Oral complications of cancer and cancer therapy: from cancer treatment to survivorship. *CA Cancer J Clin*, 2012; 62, 400–22.
- Zhang Q, Hou D, Wen XY, et al. Gold nanomaterials for oral cancer diagnosis and therapy: advances, challenges, and prospects. *Mater Today Bio*, 2022; 15, 100333.
- Li JJ, Gupta S, Li C. Research perspectives: Gold nanoparticles in cancer theranostics. *Quant Imaging Med Surg*, 2013; 3, 284–91.
- Camerin M, Rello S, Villanueva A, et al. Photothermal sensitisation as a novel therapeutic approach for tumours: studies at the cellular and animal level. *Eur J Cancer*, 2005; 41, 1203–12.
- Camerin M, Rodgers MAJ, Kenney ME, et al. Photothermal sensitisation: evidence for the lack of oxygen effect on the photosensitising activity. *Photochem Photobiol Sci*, 2005; 4, 251–3.
- He XM, Bischof JC. Quantification of temperature and injury response in thermal therapy and cryosurgery. *Crit Rev Biomed Eng*, 2003; 31, 355–422.
- Chen XJ, Zhang XQ, Liu Q, et al. Nanotechnology: a promising method for oral cancer detection and diagnosis. *J Nanobiotechnology*, 2018; 16, 52.
- Melamed JR, Edelstein RS, Day ES. Elucidating the fundamental mechanisms of cell death triggered by photothermal therapy. *ACS Nano*, 2015; 9, 6–11.
- Lei HL, Pei ZF, Jiang CY, et al. Recent progress of metal-based nanomaterials with anti-tumor biological effects for enhanced cancer therapy. *Exploration*, 2023; 3, 20220001.
- Xue XD, Qu HJ, Li YP. Stimuli-responsive crosslinked nanomedicine for cancer treatment. *Exploration*, 2022; 2, 20210134.
- Sun JY, Li JY, Li X, et al. Sequentially responsive size reduction and drug release of core-satellite nanoparticles to enhance tumor penetration and effective tumor suppression. *Chin Chem Lett*, 2023; 34, 107891.
- Hu HH, Zhang Z, Fang YF, et al. Therapeutic poly(amino acid)s as drug carriers for cancer therapy. *Chin Chem Lett*, 2023; 34, 107953.
- Zhang LP, Yang JZ, Huang J, et al. Development of tumor-evolution-targeted anticancer therapeutic nanomedicine^{EVT}. *Chem*, 2024; 10, 1337–56.
- Park S, Cho E, Chueng STD, et al. Aptameric fluorescent biosensors for liver cancer diagnosis. *Biosensors*, 2023; 13, 617.
- Wang ZH, Sun X, Huang T, et al. A sandwich nanostructure of gold nanoparticle coated reduced graphene oxide for photoacoustic imaging-guided photothermal therapy in the

- second NIR window. *Front Bioeng Biotechnol*, 2020; 8, 655.
19. Zhou RL, Zhang MG, Xi JH, et al. Gold nanorods-based photothermal therapy: interactions between biostructure, nanomaterial, and near-infrared irradiation. *Nanoscale Res Lett*, 2022; 17, 68.
 20. Dai ZY, Tan Y, He K, et al. Strict DNA valence control in ultrasmall thiolate-protected near-infrared-emitting gold nanoparticles. *J Am Chem Soc*, 2020; 142, 14023–7.
 21. Wang JW, Zhang CY, Liu Z, et al. Target-triggered nanomaterial self-assembly induced electromagnetic hot-spot generation for SERS-fluorescence dual-mode in situ monitoring MiRNA-guided phototherapy. *Anal Chem*, 2021; 93, 13755–64.
 22. Gu QF, Zhang YH, Cao HH, et al. Transfer of thiolated DNA staples from DNA origami nanostructures to self-assembled monolayer-passivated gold surfaces: implications for interfacial molecular recognition. *ACS Appl Nano Mater*, 2021; 4, 8429–36.
 23. Duan QQ, Yang M, Zhang BY, et al. Gold nanoclusters modified mesoporous silica coated gold nanorods: enhanced photothermal properties and fluorescence imaging. *J Photochem Photobiol B Biol*, 2021; 215, 112111.
 24. Liu XY, Wang JQ, Ashby CR Jr, et al. Gold nanoparticles: synthesis, physiochemical properties and therapeutic applications in cancer. *Drug Discov Today*, 2021; 26, 1284–92.
 25. Ge RL, Yan PN, Liu Y, et al. Recent advances and clinical potential of near infrared photothermal conversion materials for photothermal hepatocellular carcinoma therapy. *Adv Funct Mater*, 2023; 33, 2301138.
 26. Cheng Y, Bao DD, Chen XJ, et al. Microwave-triggered/HSP-targeted gold nano-system for triple-negative breast cancer photothermal therapy. *Int J Pharm*, 2021; 593, 120162.
 27. Ding ZF, Sigdel K, Yang L, et al. Nanotechnology-based drug delivery systems for enhanced diagnosis and therapy of oral cancer. *J Mater Chem B*, 2020; 8, 8781–93.
 28. Shan XZ, Zhao ZQ, Wang C, et al. Emerging prodrug-engineered nanomedicines for synergistic chemophototherapy. *Chem Eng J*, 2022; 442, 136383.
 29. Liu MT, Ma WJ, Zhao D, et al. Enhanced penetrability of a tetrahedral framework nucleic acid by modification with iRGD for DOX-targeted delivery to triple-negative breast cancer. *ACS Appl Mater Interfaces*, 2021; 13, 25825–35.
 30. Vázquez-González M, Willner I. Aptamer-functionalized micro- and nanocarriers for controlled release. *ACS Appl Mater Interfaces*, 2021; 13, 9520–41.
 31. Yan JQ, Zhan XH, Zhang ZZ, et al. Tetrahedral DNA nanostructures for effective treatment of cancer: advances and prospects. *J Nanobiotechnology*, 2021; 19, 412.
 32. Madkour M, Aboelenin MM, Younis E, et al. Hepatic acute-phase response, antioxidant biomarkers and DNA fragmentation of two rabbit breeds subjected to acute heat stress. *Ital J Anim Sci*, 2020; 19, 1568–76.
 33. Kara M, Oztas E. Endoplasmic reticulum stress-mediated cell death. In: Gali-Muhtasib H, Rahal O N. Programmed Cell Death. IntechOpen. 2020, 1-14.
 34. Yao F, Jin Z, Zheng ZH, et al. HDAC11 promotes both NLRP3/caspase-1/GSDMD and caspase-3/GSDME pathways causing pyroptosis via ERG in vascular endothelial cells. *Cell Death Discov*, 2022; 8, 112.
 35. Spitz AZ, Gavathiotis E. Physiological and pharmacological modulation of BAX. *Trends Pharmacol Sci*, 2022; 43, 206–20.
 36. Linder A, Bauernfried S, Cheng YM, et al. CARD8 inflammasome activation triggers pyroptosis in human T cells. *EMBO J*, 2020; 39, e105071.
 37. Hao W, Xu JS, Li YH, et al. Tetrahedral DNA nanostructure-modified gold nanorod-based anticancer nanomaterials for combined photothermal therapy and chemotherapy. *Biomed Environ Sci*, 2022; 35, 1115–25.
 38. Zhao LY, Liu YM, Xing RR, et al. Supramolecular photothermal effects: a promising mechanism for efficient thermal conversion. *Angew Chem*, 2020; 132, 3821–9.
 39. Cui XM, Ruan QF, Zhuo XL, et al. Photothermal nanomaterials: a powerful light-to-heat converter. *Chem Rev*, 2023; 123, 6891–952.
 40. Fu W, Ma L, Ju Y, et al. Therapeutic siCCR2 loaded by tetrahedral framework DNA nanorobotics in therapy for intracranial hemorrhage. *Adv Funct Mater*, 2021; 31, 2101435.
 41. Hong SB, Jiang WD, Ding QF, et al. The current progress of tetrahedral DNA nanostructure for antibacterial application and bone tissue regeneration. *Int J Nanomedicine*, 2023; 3761–80.
 42. Heuer-Jungemann A, Linko V. Engineering inorganic materials with DNA nanostructures. *ACS Cent Sci*, 2021; 7, 1969–79.
 43. Lee D, Hong JH. Activated PyK2 and its associated molecules transduce cellular signaling from the cancerous milieu for cancer metastasis. *Int J Mol Sci*, 2022; 23, 15475.
 44. Gur C, Kandemir O, Kandemir FM. Investigation of the effects of hesperidin administration on abamectin-induced testicular toxicity in rats through oxidative stress, endoplasmic reticulum stress, inflammation, apoptosis, autophagy, and JAK2/STAT3 pathways. *Environ Toxicol*, 2022; 37, 401–12.
 45. Spaas J, Van Veggel L, Schepers M, et al. Oxidative stress and impaired oligodendrocyte precursor cell differentiation in neurological disorders. *Cell Mol Life Sci*, 2021; 78, 4615–37.
 46. Qin C, Yang S, Chu YH, et al. Signaling pathways involved in ischemic stroke: molecular mechanisms and therapeutic interventions. *Signal Transduct Target Ther*, 2022; 7, 215.
 47. Carneiro BA, El-Deiry WS. Targeting apoptosis in cancer therapy. *Nat Rev Clin Oncol*, 2020; 17, 395–417.
 48. Asadi M, Taghizadeh S, Kaviani E, et al. Caspase-3: structure, function, and biotechnological aspects. *Biotechnol Appl Biochem*, 2022; 69, 1633–45.
 49. Anderton H, Wicks IP, Silke J. Cell death in chronic inflammation: breaking the cycle to treat rheumatic disease. *Nat Rev Rheumatol*, 2020; 16, 496–513.
 50. Fujimura K, Karasawa T, Komada T, et al. NLRP3 inflammasome-driven IL-1 β and IL-18 contribute to lipopolysaccharide-induced septic cardiomyopathy. *J Mol Cell Cardiol*, 2023; 180, 58–68.